ARMY RESEARCH LABORATORY

Laser-Induced Plasma Chemistry of the Explosive RDX With Various Metallic Nanoparticles

by Jennifer L. Gottfried

ARL-RP-435 **April 2013**

A reprint from *Applied Optics,* Vol. 51, No. 7, pp. B13–B21, 1 March 2012.

NOTICES

Disclaimers

The findings in this report are not to be construed as an official Department of the Army position unless so designated by other authorized documents.

Citation of manufacturer's or trade names does not constitute an official endorsement or approval of the use thereof.

Destroy this report when it is no longer needed. Do not return it to the originator.

Army Research Laboratory
Aberdeen Proving Ground, MD 21005-5069

ARL-RP-435 **April 2013**

Laser-Induced Plasma Chemistry of the Explosive RDX With Various Metallic Nanoparticles

Jennifer L. Gottfried
Weapons and Materials Research Directorate, ARL

A reprint from *Applied Optics,* Vol. 51, No. 7, pp. B13–B21, 1 March 2012.

REPORT DOCUMENTATION PAGE

Form Approved
OMB No. 0704-0188

1. REPORT DATE *(DD-MM-YYYY)*	2. REPORT TYPE	3. DATES COVERED (From - To)
April 2013	Reprint	June 2009 – September 2011

4. TITLE AND SUBTITLE
Laser-Induced Plasma Chemistry of the Explosive RDX With Various Metallic Nanoparticles

5a. CONTRACT NUMBER

5b. GRANT NUMBER

5c. PROGRAM ELEMENT NUMBER

6. AUTHOR(S)
Jennifer L. Gottfried

5d. PROJECT NUMBER

5e. TASK NUMBER

5f. WORK UNIT NUMBER

7. PERFORMING ORGANIZATION NAME(S) AND ADDRESS(ES)
U.S. Army Research Laboratory
ATTN: RDRL-WML-B
Aberdeen Proving Ground, MD 21005-5069

8. PERFORMING ORGANIZATION REPORT NUMBER
ARL-RP-435

9. SPONSORING/MONITORING AGENCY NAME(S) AND ADDRESS(ES)

10. SPONSOR/MONITOR'S ACRONYM(S)

11. SPONSOR/MONITOR'S REPORT NUMBER(S)

12. DISTRIBUTION/AVAILABILITY STATEMENT
Approved for public release; distribution is unlimited.

13. SUPPLEMENTARY NOTES
A reprint from *Applied Optics*, Vol. 51, No. 7, pp. B13–B21, 1 March 2012.

14. ABSTRACT
The feasibility of exploiting plasma chemistry to study the chemical reactions between metallic nanoparticles and molecular explosives such as cyclotrimethylenetrinitramine (RDX) has been demonstrated. This method, based on laser-induced breakdown spectroscopy, involves the production of nanoparticles in a laser-induced plasma and the simultaneous observation of time-resolved atomic and molecular emission characteristic of the species involved in the intermediate chemical reactions of the nanoenergetic material in the plasma. Using this method, it has been confirmed that the presence of aluminum promotes the ejection process of carbon from the intermediate products of RDX. The time evolution of species formation, the effects of laser pulse energy, and the effects of trace metal content on the chemical reactions were also studied.

15. SUBJECT TERMS
LIBS, RDX, plasma chemistry, metallic nanoparticles

16. SECURITY CLASSIFICATION OF:			17. LIMITATION OF ABSTRACT	18. NUMBER OF PAGES	19a. NAME OF RESPONSIBLE PERSON
a. REPORT	b. ABSTRACT	c. THIS PAGE			Jennifer L. Gottfried
Unclassified	Unclassified	Unclassified	UU	14	19b. TELEPHONE NUMBER (*Include area code*) 410-278-7573

Laser-induced plasma chemistry of the explosive RDX with various metallic nanoparticles

Jennifer L. Gottfried

U.S. Army Research Laboratory, RDRL-WML-B, Aberdeen Proving Ground, Maryland, 21005, USA (jennifer.gottfried@us.army.mil)

Received 27 September 2011; revised 10 January 2012; accepted 13 January 2012; posted 13 January 2012 (Doc. ID 155400); published 26 January 2012

The feasibility of exploiting plasma chemistry to study the chemical reactions between metallic nanoparticles and molecular explosives such as cyclotrimethylenetrinitramine (RDX) has been demonstrated. This method, based on laser-induced breakdown spectroscopy, involves the production of nanoparticles in a laser-induced plasma and the simultaneous observation of time-resolved atomic and molecular emission characteristic of the species involved in the intermediate chemical reactions of the nanoenergetic material in the plasma. Using this method, it has been confirmed that the presence of aluminum promotes the ejection process of carbon from the intermediate products of RDX. The time evolution of species formation, the effects of laser pulse energy, and the effects of trace metal content on the chemical reactions were also studied.

OCIS codes: 140.3450, 300.6365.

1. Introduction

It is well known that two-component explosives consisting of metal particle fuels and oxidizers can produce more than twice the energy of high performance molecular explosives alone. Aluminum powder (typically ~50 μm average diameter) is frequently added to explosives and propellants to improve their performance. The addition of metallic aluminum results in a considerable increase in the heat of explosion and higher temperatures since alumina (Al_2O_3) has a high heat of formation [1]. Other fuels used in heat-producing pyrotechnics include Ti, Mg, Ni, Zr, and Be [2]. Recently there has been considerable interest in using nanoparticle fuels, which offer the possibility of faster energy release, more efficient combustion, and controllable explosive performance (via particle size or passivation layer properties) [3,4]. The development of nanoenergetic materials has been limited by the lack of fundamental understanding regarding the chemical dynamics involved.

The need to understand the chemical mechanisms of combustion, thermal explosion, and detonation is essential in order to develop more efficient explosives and propellants. In addition, the chemical products produced during detonation can negatively affect device performance, so an understanding of the chemical reactions involved during the decomposition of component mixtures is crucial. In a recent study, Song *et al.* investigated the formation of C and AlO in an aluminized-cyclotrimethylenetrinitramine (RDX) shock tube explosion [5]. Both unreacted carbon (C, C_2) and AlO decrease rocket performance. By monitoring the C_2 and AlO emission, they observed that increasing the quantity of Al particles (~4.5 μm diameter) added to the RDX resulted in increased C_2 emission. They subsequently studied the effect of nanoaluminum on the detonation of RDX in a similar experimental setup [6].

Here, we demonstrate an alternate approach for studying the chemical reactions of molecular explosives and metallic nanoparticles. This approach, based on laser-induced breakdown spectroscopy (LIBS), involves generating the metallic nanoparticles via laser ablation and studying the chemical reactions that occur in the laser-induced plasma by monitoring the time-resolved emission spectra. In the past decade, laser ablation has increasingly been used to produce metallic nanoparticles. The size and distribution of the nanoparticles can be controlled by using sequential laser pulses, varying repetition rates, laser fluence, wavelength, and pulse width,

and choice of carrier gas (air, argon, nitrogen, etc.) [7–10]. LIBS is an analytical technique that has been widely investigated over the past several decades for both qualitative and quantitative material analysis [11]; previous applications include the detection of explosives [12]. It is only recently that a few groups have started investigating the chemical reactions involving explosive materials that occur during the lifetime of the laser-induced plasma (tens to hundreds of microseconds) and the subsequent effect on the LIBS signature [13–18].

The potential advantages to this approach to studying nanoenergetic materials include (1) little or no sample preparation is needed (the laser directly ablates the explosive and substrate material), (2) the intermediate chemical reactions of the nanoenergetic material can be studied on a small scale (microgram quantities), eliminating the need for a shock tube or other explosive containment apparatus, (3) the properties of the laser (pulse energy, wavelength, pulse duration) can be tuned to control the size and distribution of the particles formed, and (4) time-resolved relative concentrations of a large number of atomic and molecular species can be tracked simultaneously. With this approach, any type of material can be ablated with the laser and its plasma chemistry studied as long as the laser energy exceeds the breakdown threshold.

In this work, the laser ablation of thin film residues of RDX on various metal substrates (generating nanoenergetic particles) has been combined with the observation of time-resolved optical emission from the resulting high-temperature plasma. The relative concentrations of C, C_2, CN, H, N, and O (as well as any other metal substrate-related atomic, molecular, or ionic species emitting from 200–940 nm) were tracked during the lifetime of the plasma (typically <1 ms). Several experiments designed to understand the time dependence of species formation in the plasma, to determine the effect of bulk and trace metals on the chemistry of RDX, and to study the effects of laser pulse energy were performed.

2. Experimental Methods

Colleagues at the U.S. Army Research Laboratory provided Class 1 (<850 μm particle diameter), military-grade RDX. Double pulse LIBS spectra of a thin layer of RDX crushed on the surface of a 1-mm-thick Al substrate (Sigma-Aldrich, 99.999%) were obtained using two Big Sky CFR400 lasers (1064 nm, 225 mJ per laser) focused on the sample surface with a 10 cm focal length convex lens. The interpulse delay between the two laser pulses ($\Delta t = 2$ μs) was selected to minimize the amount of atmospheric contribution to the O, N, and H emission signals. A pierced mirror was used to collect the spatially integrated plasma emission in a 600 μm fiber optic. The fiber was inserted into a Catalina Scientific echelle spectrometer (SE200) through a 25 μm pinhole (200–1000 nm). An Apogee (AP2Ep) ICCD (gain = 600) served as the detector. The gate delay (t_{delay}) was varied from 0 to 10 μs while the integration time ($t_{\text{int}} = 1$ μs) was held constant at the minimum value for the detector. Ten single-shot spectra at each gate delay were recorded.

To study the laser-induced plasma chemistry, a second double pulse LIBS setup was employed. For this experiment, two Nd:YAG lasers (Continuum Surelite, 1064 nm, maximum $\simeq$420 mJ per laser) were focused onto the sample surface with a 10 cm lens. The plasma emission was directed into a 400 μm fiber optic using a pierced mirror setup. An echelle spectrometer (Catalina Scientifc EMU-65) was paired with an electron multiplying CCD (EMCCD) detector (Andor iXon, gain = 2) to collect the LIBS spectra (200–1000 nm) under an argon flow with the following timing parameters: $\Delta t = 2$ μs, $t_{\text{int}} = 50$ μs, and $t_{\text{delay}} = 1$ μs. Both detectors [intensified CCD (ICCD) and EMCCD] were corrected for their spectral responses using a calibrated deuterium tungsten–halogen light source. For the samples used to study the plasma chemistry, the RDX was suspended in acetonitrile, which enables fairly reproducible, semiquantitative sample deposition. Typical RDX concentrations of $\sim$10 mg/ml were applied to the substrate surfaces with multiple deposits from a 10 μl syringe, resulting in residue concentrations of $\sim$2.5 μg/mm^2; approximately 13 μg of RDX was sampled with each laser shot. The substrates used for this experiment were high-purity metals ($\geq$1 mm thick) obtained from Sigma-Aldrich: Al (99.999%), Cu (99.999%), Ni (99.98%), Sn (99.998%), and Ti (99.998%). Fifty single-shot spectra of RDX residue on each of the pure metal substrates were obtained. Spectra of RDX residue on an Al_2O_3 sample from our laboratory and Al alloy standard reference material (SRM) purchased from the National Institutes of Standards and Technology (NIST SRM 1256b, alloy 380; NIST SRM 1259, alloy 7075; NIST SRM 1715, alloy 5182) were also acquired.

Additional experiments performed using the Continuum double pulse laser setup include the sampling of mixtures of RDX with <75 μm diameter Al powder (Sigma-Aldrich). The Al powder was added to 8 mg of RDX in several weight ratios (0:1, 1:1, 2:1, and 4:1). The mixtures were then spread onto a 6.5 cm^2 area on the surfaces of the pure metal substrates Al, Cu, Ni, Sn, and Ti. Fifteen single-shot spectra were acquired under argon for each sample. Unlike the pure RDX residue, which tends to stick easily to substrate surfaces, a significant portion of the RDX/Al mixtures was blown off the substrate by the shock wave from each laser shot. An exhaust port was placed near the point of laser ablation to ensure none of the explosive mixtures were inhaled or otherwise dispersed into the laboratory.

The dependence of the emission spectra on laser pulse energy was studied using the Continuum double pulse laser with the echelle/EMCCD spectrometer. As before, the RDX was suspended in acetonitrile and deposited on the pure Al substrate

(~2.5 $\mu g/mm^2$). Twenty spectra of both the pure substrate and the RDX residue were acquired under argon using a single 210 mJ laser pulse, a double 210 mJ pulse (total energy 420 mJ), a single 420 mJ pulse, and a double 420 mJ pulse (total energy 840 mJ).

3. Results and Discussion

A. Time-Resolved Emission Spectroscopy

Background-corrected peak emission intensities for the atomic and molecular species relevant to RDX were tracked over the first 10 μs of the laser-induced plasma lifetime (Fig. 1). Although the emission spectra collected with a 0 μs gate delay (and a 1 μs gate width) contain the background continuum characteristic of *bremsstrahlung* emission (which persists for the first several hundred nanoseconds), discrete emission lines were also observed. After subtracting the average background signal near the relevant emission line, the peak intensities for the C (247.856 nm), H (656.285 nm), N (746.831 nm), and O (777.194/777.417 nm) lines were normalized to the total emission intensities of selected atomic and molecular species, including CN (388.340 nm), C_2 (516.520 nm), and AlO (484.220 nm). Because the RDX residue was applied to an aluminum substrate, Al I and Al II emission features were observed in addition to AlO (formed by the reaction of the Al from the substrate and O liberated from the RDX).

The cause of the initial increase in the normalized O intensity over the first several microseconds is unclear, but may be the result of slower dissociation reactions involving the release of atomic O. The O (after 2 μs), N, and H emission from the RDX slowly decays over time, while the C emission is relatively constant for the first 10 μs of the plasma lifetime. The energy required to promote C into the excited state (which subsequently emits radiation at 247.856 nm as the electron relaxes to a lower energy level) is much lower than that for the O, N, and H lines (7.68 eV compared to 10.7 , 12.0, and 12.1 eV, respectively) [19] and is therefore less affected by the decreasing thermal energy in the plasma at later times. Because the double pulse LIBS technique [20] was used to collect the data, only a minimal amount of air was entrained into the plasma and most of the O, N, and H signals were from the RDX residue (and potentially contaminants on the aluminum surface).

As previously reported for other materials with much lower laser energies [21–23], the molecular species exhibit very different time-dependent behavior in the laser-induced plasma. Of the three molecules observed in the LIBS spectra of RDX on aluminum, only the CN is present at very early times in the plasma lifetime since some CN fragments are formed by the initial laser ablation of the RDX molecule (Figure 2). These initial CN fragments are dissociated into atomic C and N atoms by collisions in the high-temperature plasma [13]. The ratio of singly ionized Al (466 nm) to neutral Al (309 nm) is also shown in Fig. 2. The excitation temperatures calculated based on the Boltzmann two-line method using the Al I lines (309 and 394 nm) follow the same trend as the ionization ratio—both decrease as the plasma cools. The calculated temperatures drop from ~11,000 K at a gate delay of 0 μs to around 3700 K at a gate delay of 10 μs. As the plasma begins to cool, CN, C_2 and AlO form from chemical reactions, e.g., Eqs. (1–4) [13], Eq. (5) [24], and Eq. (6) [25], resulting in an increase in molecular emission at times >2 μs:

$$C + N + M \rightarrow CN + M, \quad (1)$$

$$C + N_2 \rightarrow CN + N, \quad (2)$$

$$CO + C \rightarrow C_2 + O, \quad (3)$$

$$CN + C \rightarrow C_2 + N, \quad (4)$$

$$Al + O + M \rightarrow AlO + M, \quad (5)$$

$$Al + CO_2 \rightarrow AlO + CO. \quad (6)$$

The formation of molecular species during the lifetime of the laser-induced plasma is clear evidence

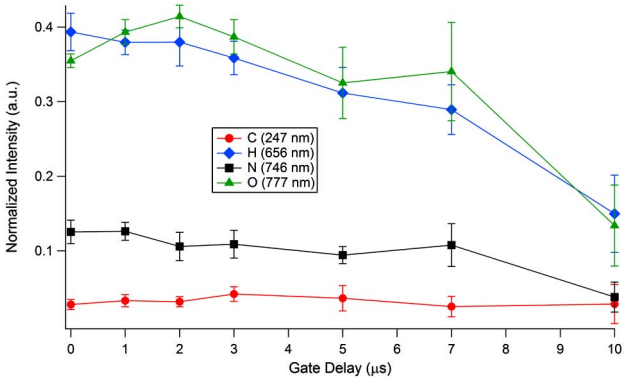

Fig. 1. (Color online) Peak atomic emission intensities as a function of gate delay (gate width 1 μs). Error bars represent 95% confidence intervals.

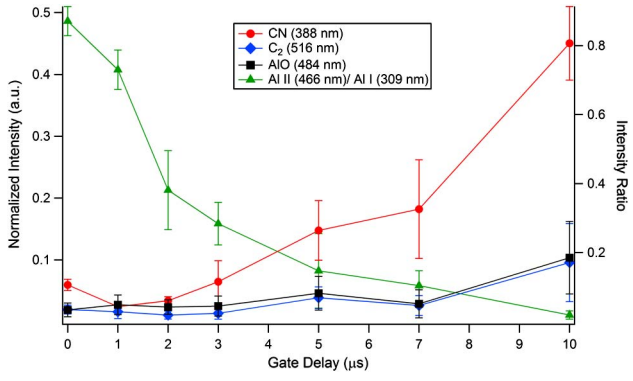

Fig. 2. (Color online) CN, C_2, and AlO emission (shown as a function of gate delay with a gate width = 1 μs) increases as the plasma cools and becomes less ionized. Error bars represent 95% confidence intervals.

that chemistry is occurring in the highly excited, nonequilibrium environment. While most LIBS practitioners therefore limit the detector gate width in order to minimize changes in the emission intensities (at the expense of sensitivity), our goal was to determine if useful information about the species involved in the plasma chemistry can be obtained using longer gate widths. While using longer gate widths results in stronger overall emission intensities, changes in emission intensities resulting from chemical reactions in the plasma (as well as changes in the plasma temperature) also affect the relative emission intensities for the different species in the plasma over the integrated plasma lifetime.

B. Plasma Chemistry

Selected regions of spectra (double pulse LIBS under argon) from the five high-purity substrates with and without RDX are shown in Figure 3. The increase in the C, H, N, O, and CN emission with the presence of RDX (dotted red traces) is clearly visible. In this experiment very little air was entrained in the laser-induced plasma, so most of the nitrogen used in the formation of CN originates from the RDX. The highest excitation temperatures for the RDX/metal plasmas (calculated using the Ar I lines at 750.387 and 751.465 nm) correspond to Ti > Al > Cu > Sn > Ni (Table 1). The Ti substrate plasma had the greatest increase in temperature with the addition of RDX, while the plasma for the Sn substrate remained essentially unchanged. The higher plasma temperature for the blank Sn implies less laser energy coupled to the sample and more energy went into heating the plasma. In this case, there would be fewer ablated Sn atoms in the plasma to affect the chemistry.

The extent of ionization for each RDX/metal plasma (represented by the ion/neutral ratio) followed almost the same trend as the temperature, Ti > Al > Cu > Ni > Sn (Fig. 4). The ion/neutral ratios are drastically different among the substrates. Al and Ti have the lowest ionization potentials of the five substrates (5.986 and 6.828 eV, respectively, compared to 7.726 eV for Cu, 7.640 eV for Ni, and 7.344 eV for Sn) [26], and their plasmas have the highest ion/neutral ratios. The ionization of the Al plasma is substantially decreased when RDX residue is added to the substrate, while the ionization in the Ti and Cu plasmas increased. The ionization of the Ni and Sn substrate plasmas showed little change with the addition of RDX residue. These properties of the substrate will significantly affect the chemical reactions occurring in the laser-induced plasma.

Table 1. Calculated Excitation Temperatures for Metal Substrates With and Without RDX Residue

	Temperature (K)		
Substrate	Blank	RDX Residue	% Change
Al	9594 ± 251	12195 ± 796	27%
Cu	9369 ± 142	11802 ± 611	26%
Ni	9839 ± 177	11335 ± 488	15%
Sn	11639 ± 398	11434 ± 585	–1.8%
Ti	9123 ± 176	16834 ± 1295	85%

Figure 5 shows three contour plots created by plotting the relative emission intensities of species within the laser-induced plasma (normalized to the Ar line at 763.511 nm) generated by ablation of RDX residue on the five substrates. These plots illustrate the variations in the plasma chemistry caused by the different substrates. Figure 5(a) shows that, as the C intensity in the plasma increases, the CN intensity increases, as well. The CN intensity is essentially independent of the atomic N content, however, which indicates that Eq. (2) is the dominant mechanism for formation of CN in the plasma, rather than Eq. (1). This observation is consistent with previous results (e.g., [23]). The O intensity increases as the N increases, while increasing C content results in decreasing O [Fig. 5(b)]. This result can be explained by the formation of CO and CO_2 in the plasma via the reactions

$$C + O + M \rightarrow CO + M, \tag{7}$$

$$CO + O \rightarrow CO_2. \tag{8}$$

Equations (7) and (8) are important reactions in the decomposition of RDX, since the formation of gaseous

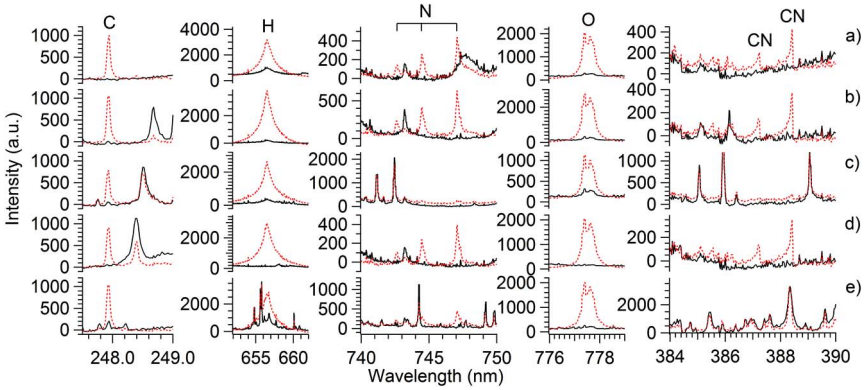

Fig. 3. (Color online) Selected regions of LIBS spectra for (a) Al, (b) Cu, (c) Ni, (d) Sn, and (e) Ti with (dotted red) and without (solid black) RDX residue.

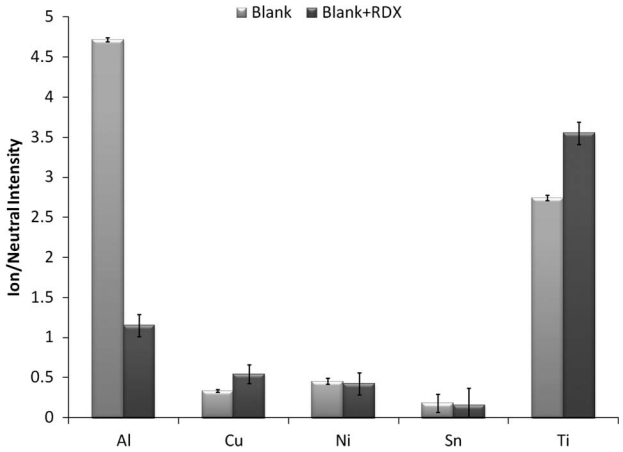

Fig. 4. Ion/neutral intensity ratios for the five high-purity substrates with and without RDX residue. The Al I 669.867 nm and Al II 466.306 nm lines were used to calculate ion/neutral ratios for Al since the 309.271 nm line was saturated. Other emission lines used for calculating ion/neutral ratios included: Cu I 296.116 nm and Cu II 227.626 nm, Ni I 343.356 nm and Ni II 243.789 nm, Sn I 333.062 nm and Sn II 533.236 nm, Ti I 373.890 nm and Ti II 462.928 nm. Error bars represent 95% confidence intervals.

products such as CO and CO_2 is highly exothermic and results in the liberation of large quantities of energy upon detonation [27]. Figure 5(c) shows that, as the CN intensity increases, the O intensity decreases. This decrease in O content in the presence of CN can be explained by the reaction

$$CN + O \rightarrow CO + N. \quad (9)$$

The concentration of atomic O in the laser-induced plasma is, therefore, highest in conditions of low C and low CN.

The assumption for the preceding analysis is that the minor differences in plasma temperature between substrates with RDX residue on them (with the exception of Ti, see Table 1) are less important than the effects of the ablated metal on the plasma chemistry. Since the subsequent analysis agrees with previous studies, we believe this assumption is reasonable. For a more quantitative approach to this analysis, inclusion of the temperature and ground state populations would need to be considered. In addition, the plasma chemistry is extremely complex, and there may be further complications not considered in this simplified approach.

To further understand the effect of metals on the chemical reactions of RDX in the laser-induced plasma, Al powder was mixed with the RDX in varying concentrations (0∶1, 1∶1, 2∶1, and 4∶1) and applied to the five substrates. Al is rapidly oxidized by oxygen (O, O_2), CO_2, H_2O, and possibly other species, such as NO, N_2O, and NO_2, to form AlO before reaching its final equilibrium state, alumina (Al_2O_3) [28]. Because of the high heat of formation for Al_2O_3, the addition of Al to explosive formulations results in a considerable increase in the heat of explosion. In

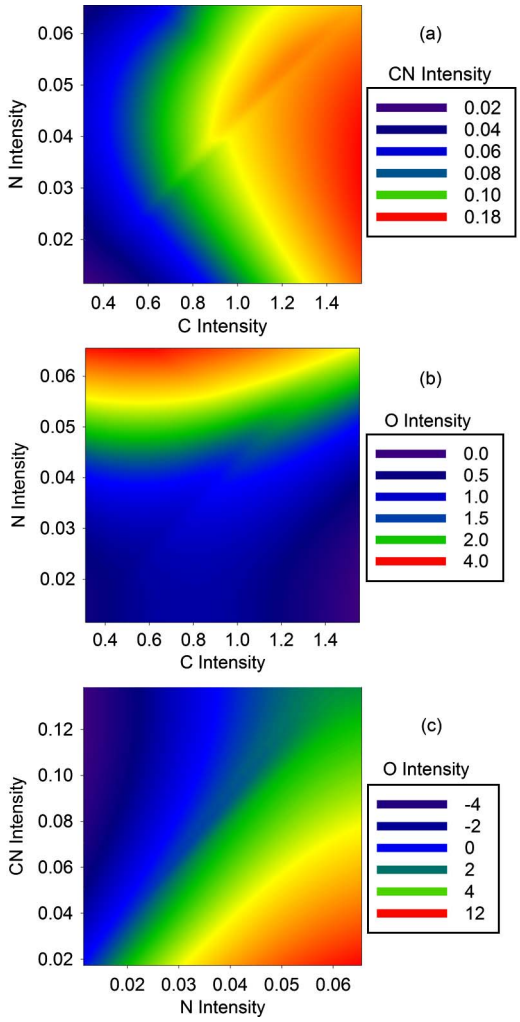

Fig. 5. (Color online) Contour plots for the (a) N, C, CN, (b) N, C, O, and (c) CN, N, O emission intensities of RDX on five different metal substrates (Al, Cu, Ni, Sn, and Ti).

these experiments, the laser-induced plasma temperature for each substrate increased by as much as 55% with the addition of Al powder to the RDX (Fig. 6). The Ti was the only substrate that showed an initial decrease in plasma temperature with Al (compared to the pure RDX residue).

As the concentration of Al powder was increased, the substrate emission lines decreased (due to increased residue surface coverage) and the Al emission lines increased. While the C, H, N, H, and CN emission lines decreased with increasing Al (possibly because less RDX was being sampled in the plasma), the C_2 and AlO increased on all substrates (Fig. 7). This result is confirmed by the conclusions of Song *et al.* [5], who observed the increase in C_2 and AlO emission with increasing Al content during an aluminized-RDX explosion in a shock tube. The higher the concentration of Al in the laser-induced plasma, the more O the Al scavenges to form AlO, and the less O available to react with the C to form CO. This results in an increase in condensed phase C aggregate (soot) and C_2. Although the increase in

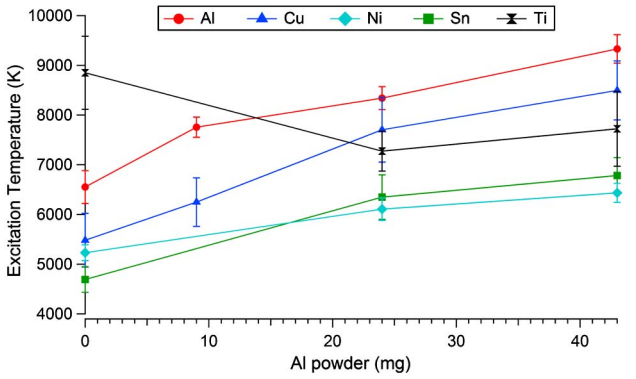

Fig. 6. (Color online) Excitation temperatures for RDX/Al mixture residues on Al, Cu, Ni, Sn, and Ti substrates calculated using Al I lines at 308.215 and 396.152 nm. Error bars represent 95% confidence intervals.

plasma temperature is more significant in this set of experiments, the accumulation of soot with increasing Al content has been observed in the previous experiment [5], substantiating our assumption that the increase in C_2 emission results from chemical reactions in the plasma.

C. Laser Pulse Energy Dependence

Conventional formulations of energetic materials containing Al particles to improve the performance of explosives and propellants use particles with a mean diameter of ~50 μm, but the reactivity of Al nanoparticles has been shown to increase with decreasing size [29]. Previous experiments have demonstrated that ablation of an Al target with a pulsed laser produces Al nanoparticles with a mean primary particle size of 5–500 nm (depending on laser pulse duration and fluence as well as carrier gas type and pressure) [7,9,30]. It has also been demonstrated that using higher laser pulse energies increases the number of smaller nanoparticles produced [10].

A comparison of the LIBS spectra of RDX on Al obtained using different pulse energy schemes (ranging from 210 to 840 mJ) showed that higher laser pulse energy results in both increased overall spectral emission and relative AlO emission (Fig. 8); the smaller Al particle sizes produced by the high laser pulse energy are more reactive (due to the higher relative surface area) and, therefore, are oxidized more quickly. While the slight increase in plasma temperature observed with increasing laser pulse energy affects the observed emission intensities, the standard deviation for the calculated temperatures was only 505 K, so we would expect this effect to be minimal.

The double laser pulses result in stronger RDX spectra (compared to single pulse spectra of the same total pulse energy), but weaker AlO emission, since less O is entrained in the laser-induced plasma (as seen by comparing the O intensity from the blank Al at 420 mJ versus 2 × 210 mJ in Fig. 8). The relative C intensity increases with increasing laser pulse energy. Unlike with the AlO, there is no decrease in C emission between a single 420 mJ pulse and a double

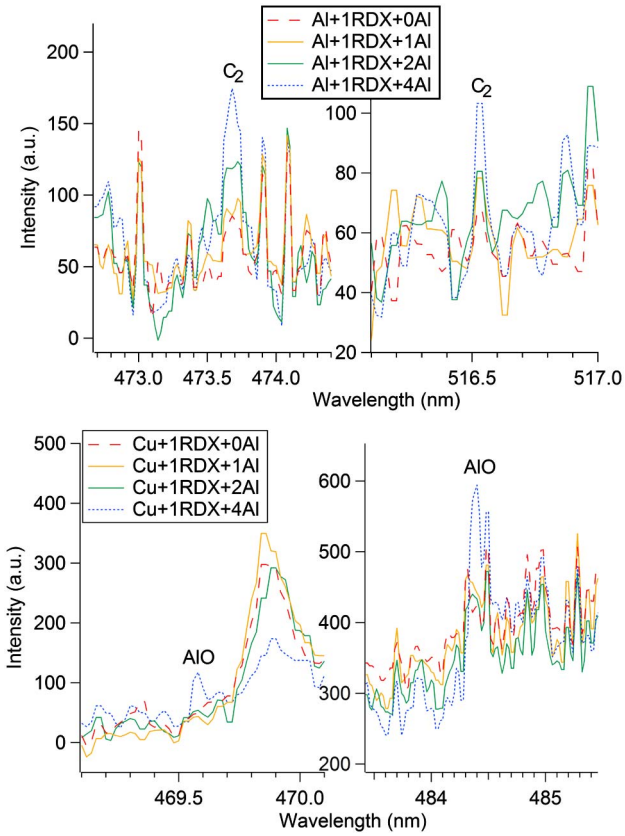

Fig. 7. (Color online) As the concentration of Al in the RDX/Al mixture was increased, the C_2 (top) and AlO (bottom) emission from the laser-induced plasma increased on all five metal substrates, including the Al and Cu substrates.

2 × 210 mJ pulse. Despite the strong C signal, no C_2 was observed at any laser pulse energy. RDX does not contain any C—C bonds, so no C_2 fragments are formed by the initial laser ablation (Fig. 2). Without the presence of additional Al to scavenge the O, the O in the plasma reacts with C (Eq. 7), preventing the formation of significant amounts of C_2 [15].

D. Effect of Trace Elements on RDX Chemistry

In addition to studying the interaction of pure metal substrates and Al additive with RDX, we also investigated the effect of minor impurities or trace elements on the chemical reactions occurring in the laser-induced plasma. LIBS spectra of a series of primarily aluminum samples were obtained, including an Al_2O_3 substrate and three NIST standard reference material Al alloys. Table 2 lists the concentrations of the trace elements for each sample (when known), divided into two categories: those observed in the double pulse LIBS spectra in argon, and those that were not observed. Only the Al_2O_3 substrate spectra contained significant O emission lines, indicating that the atmospheric contributions to the LIBS signal were negligible (none of the blank substrates had measurable N lines). All five substrates have C and H lines, even after multiple cleaning shots to remove surface contamination.

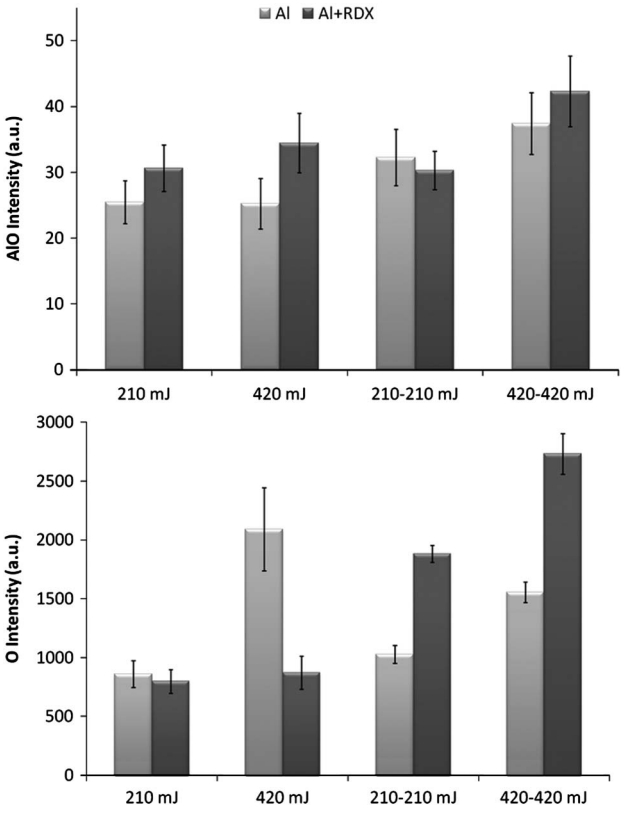

Fig. 8. Emission intensity for AlO (top) and O (bottom) obtained from RDX residue on Al with a single 210 mJ pulse, a 420 mJ pulse, and double pulse excitation (2×210 and 2×420 mJ). Error bars represent 95% confidence intervals.

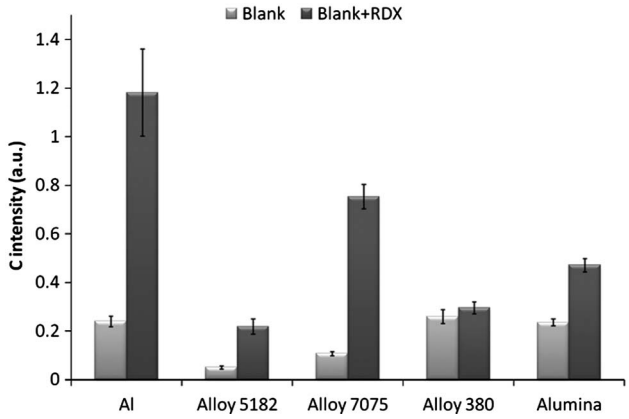

Fig. 9. Emission intensities for the C line from the LIBS spectra of RDX residue on five different Al samples. Error bars represent 95% confidence intervals.

RDX residue was applied to the five aluminum substrates and Fig. 9 shows the C emission intensities (normalized to the Ar line at 763.511 nm) observed in the LIBS spectra. The high-purity aluminum substrate, with the fewest trace elements, gave the strongest C signal from the RDX residue. The presence of more Al in the plasma increases the C signal by reducing the amount of free O available to react with C via Eq. (7). However, much of this increase in C emission intensity can be attributed to the higher plasma temperature with the pure Al substrate ($12{,}086 \pm 356$ K). The four Al alloys, on the other hand, produce nearly identical plasma temperatures when the RDX residue is present (within the standard deviation of the shot-to-shot variation). For example, alloy 5182 (with RDX) results in a plasma temperature of $10{,}565 \pm 145$ K, compared to $10{,}608 \pm 243$ K for alloy 7075—yet the increase in C emission signal is nearly fourfold for alloy 7075. Differences in the plasma chemistry resulting from the trace elements present in the aluminum alloys are clearly evident. Alloy 7075 has the highest Zn concentration, and the highest C signal of the three alloys. Alloy 5182, despite having the highest Al concentration of the three alloys, has the highest Mg concentration. Since Zn has a significantly lower oxidation potential (0.76 V) than Mg (2.37 V) [26], it makes sense that alloy 7075 would have the highest C signal among the alloys and alloy 5182 would have the lowest—the presence of easily oxidizable species will decrease the amount of O available to react with the C. Alloy 380 also contains a significant amount of Si, which also has a low oxidation potential (0.91 V) [26]. Alumina has the highest O content, which would typically favor the formation of CO/CO_2 (i.e. less C emission); however, this effect may be offset by its higher aluminum content than the other three alloy substrates.

4. Conclusions

Although, at first glance, an explosive detonation and a laser-induced plasma may not seem to have much in

Table 2. Trace Metal Content (Including Elements Observed in LIBS Spectra) for Five Different Aluminum Samples

		Minor Components	
Sample	% Al	Observed	Not Observed
Alumina (Al_2O_3)	unknown	Si, Mg, Fe, Ti, Sr, Cr, Pb, Cu	Mn, Zn, Ni, Sn, Be
Alloy 380	82.99	9.362% Si, 3.478% Cu, 1.011% Zn, 0.865% Fe, 0.3857% Mn, 0.4135% Ni, 0.0188% Sr, 0.877% Ti, 0.0572% Cr, 0.0637% Mg, 0.1075% Pb, 0.0212% V	0.35% Sn
Alloy 7075	89.76	5.44% Zn, 2.48% Mg, 1.60% Cu, 0.025% Be, 0.173% Cr, 0.18% Si, 0.205% Fe, 0.079% Mn, 0.063% Ni	
Alloy 5182	94.58	4.474% Mg, 0.3753% Mn, 0.1553% Si, 0.0494% Cu, 0.199% Fe	0.034% Cr, 0.015% Pb, 0.0195% Ni, 0.0002% Sr, 0.0335% Ti, 0.0174% V, 0.0505% Zn
Aluminum	99.999	Si, Cu, Fe	Mn, Zn, Sn, Pb, Ni, Sr, Ti, Cr, V, Be

common, they are both very high-temperature (thousands of Kelvin), high pressure (up to ~10^5 atm) environments subjected to a shock wave resulting in the rapid decomposition of the explosive into atomic constituents and subsequent exothermic formation of gaseous products. Understanding the chemistry that occurs in the reaction front of an explosive detonation is extremely difficult due to the short time scale and violent release of energy in the form of heat, sound, light, and blast. In addition, full-scale detonation testing is quite expensive. The ability to study the chemical reactions of explosives in a small-scale laboratory environment that does not require extensive safety precautions would greatly benefit the development of improved explosive formulations. The use of optical emission spectroscopy to study the chemical reactions of laser-generated nanoenergetic materials in laser-induced plasmas is extremely promising. By monitoring the emission intensity of different reactant species as a function of time, a better understanding of the chemistry of metallic nanoparticles and molecular explosives at high temperatures can be achieved, eventually enabling the development of explosive formulations with higher explosive power and fewer harmful byproducts.

Time-resolved, broadband emission of chemical species involved in the reaction of RDX and metallic nanoparticles in a laser-induced plasma has been observed. Using the methodology presented here for investigating the chemical processes involved in nanoenergetic material reactions, we observed the increase in C_2 emission resulting from an increase in Al powder additive, as confirmed by the observations of Song *et al.* [5] in a shock tube explosion. The time evolution of species formation, the effects of laser pulse energy, and the effects of trace metal content on chemical reactions were also studied. In addition to matrix effects induced by the interaction of the laser with the metal substrate (affecting the amount of material ablated, plasma temperatures, electron densities, etc.), we have shown that differences in the plasma chemistry of RDX with ablated metals significantly alters the LIBS spectra of RDX.

In a recent kinetic modeling study by Ma and Dagdigian [23], the effect of Al particles ablated from the substrate surface on the plasma chemistry was neglected based on assumptions as to the entrainment of the ablated Al in the laser-induced plasma [16]. Their initial experimental results [16], which formed the basis for this assumption, were obtained under very different experimental conditions than the present study (a single laser pulse of 20 mJ at 355 nm on a thin Al foil was used). In addition, the effect of the presence of organic residue on the laser–material interaction was not considered. Their resulting kinetic model significantly underestimated the molecular emission of C_2 (and CN) from the plasma [23]. Our current experimental results showing that increasing the Al content in the plasma results in increased C_2 emission as a result of the preferential oxidation of Al over C suggest that including the effects of Al in the kinetic model may improve the results.

Future improvements to the current experimental setup should include the incorporation of on-line monitoring of particle size distribution [10] in order to directly correlate the plasma chemistry to particle size effects, and the monitoring of mid-IR emission from the plasma to obtain information on the concentration of important species such as CO, CO_2, NO, and NO_2 in the plasma [31]. Experiments are underway to study the particle sizes produced by laser ablation of RDX. Additional experiments to be performed include tuning the laser properties, such as pulse duration and wavelength, to adjust the size and size distribution of the ablated particles, and exploring other explosive formulations, such as TNT/Al and Al/Teflon.

The author thanks Dr. Frank C. De Lucia, Jr. for numerous thoughtful discussions relating to this work.

References

1. P. Politzer, P. Lane, and M. E. Grice, "Energetics of aluminum combustion," J. Phys. Chem. A **105**, 7473–7480 (2001).
2. P. W. Cooper and S. R. Kurowski, *Introduction to the Technology of Explosives* (Wiley-VCH, 1996).
3. P. Brousseau and C. J. Anderson, "Nanometric aluminum in explosives," Propellants Explos. Pyrotech. **27**, 300–306 (2002).
4. D. D. Dlott, "Thinking big (and small) about energetic materials," Mater. Sci. Technol. **22**, 463–473 (2006).
5. Y. Song, J.-H. Wu, Y.-P. Wang, G.-D. Wu, and X.-D. Yang, "Optical investigation of shock-produced chemical products in pseudo-aluminized explosive powders explosion," J. Phys. D **40**, 3541–3544 (2007).
6. Y. Song, J.-H. Wu, M.-A. Xue, Y.-P. Wang, D. Hu, and X.-D. Yang, "Spectral investigations of the combustion of pseudo-nanoaluminized micro-cyclic-$[CH_2N(NO_2)]_3$ in a shock wave," J. Phys. D **41**, 235501 (2008).
7. M. Ullmann, S. K. Friedlander, and A. Schmidt-Ott, "Nanoparticle formation by laser ablation," J. Nanopart. Res. **4**, 499–509 (2002).
8. S. Eliezer, N. Eliaz, E. Grossman, D. Fisher, I. Gouzman, Z. Henis, S. Pecker, Y. Horovitz, M. Fraenkel, S. Maman, and Y. Lereah, "Synthesis of nanoparticles with femtosecond laser pulses," Phys. Rev. B **69**, 144119 (2004).
9. S. Amoruso, R. Bruzzese, M. Vitiello, N. N. Nedialkov, and P. A. Atanasov, "Experimental and theoretical investigations of femtosecond laser ablation of aluminum in vacuum," J. Appl. Phys. **98**, 044907 (2005).
10. R. Sattari, C. Dieling, S. Barcikowski, and B. Chichkov, "Laser-based fragmentation of microparticles for nanoparticle generation," J. Laser Micro/Nanoeng. **3**, 100–105 (2008).
11. D. A. Cremers and L. J. Radziemski, *Handbook of Laser-Induced Breakdown Spectroscopy* (Wiley, 2006).
12. J. L. Gottfried, F. C. De Lucia Jr., C. A. Munson, and A. W. Miziolek, "Laser-induced breakdown spectroscopy for detection of explosives residues: a review of recent advances, challenges, and future prospects," Anal. Bioanal. Chem. **395**, 283–300 (2009).
13. V. I. Babushok, F. C. DeLucia, P. J. Dagdigian, J. L. Gottfried, C. A. Munson, M. J. Nusca, and A. W. Miziolek, "Kinetic modeling study of the laser-induced plasma plume of cyclotrimethylenetrinitramine (RDX)," Spectrochim. Acta Part B **62**, 1321–1328 (2007).
14. V. Lazic, A. Palucci, S. Jovicevic, C. Poggi, and E. Buono, "Analysis of explosive and other organic residues by laser

induced breakdown spectroscopy," Spectrochim. Acta Part B **64**, 1028–1039 (2009).
15. F. C. De Lucia, Jr. and J. L. Gottfried, "Characterization of a series of nitrogen-rich molecules using laser-induced breakdown spectroscopy," Propellants Explos. Pyrotech. **35**, 268–277 (2010).
16. P. J. Dagdigian, A. Khachatrian, and V. I. Babushok, "Kinetic model of C/H/N/O emissions in laser-induced breakdown spectroscopy of organic compounds," Appl. Opt. **49**, C58–C66 (2010).
17. P. Lucena, A. Dona, L. M. Tobaria, and J. J. Laserna, "New challenges and insights in the detection and spectral identification of organic explosives by laser induced breakdown spectroscopy," Spectrochim. Acta Part B **66**, 12–20 (2011).
18. M. Civiš, S. Civiš, K. Sovová, K. Dryahina, P. Španél, and M. Kyncl, "Laser ablation of FOX-7: proposed mechanism of decomposition," Anal. Chem. **83**, 1069–1077 (2011).
19. Y. Ralchenko, A. E. Kramida, J. Reader, and N. A. Team, "NIST atomic spectra database (version 4.1)" (National Institute of Standards and Technology, 2010), retrieved 6 Sept. 2011, http://physics.nist.gov/asd.
20. V. I. Babushok, F. C. De Lucia Jr., J. L. Gottfried, C. A. Munson, and A. W. Miziolek, "Double pulse laser ablation and plasma: laser induced breakdown spectroscopy signal enhancement," Spectrochim. Acta Part B **61**, 999–1014 (2006).
21. M. Baudelet, M. Boueri, J. Yu, S. S. Mao, V. Piscitelli, X. Mao, and R. E. Russo, "Time-resolved ultraviolet laser-induced breakdown spectroscopy for organic material analysis," Spectrochim. Acta Part B **62B**, 1329–1334 (2007).
22. M. Boueri, M. Baudelet, J. Yu, X. L. Mao, S. S. Mao, and R. Russo, "Early stage expansion and time-resolved spectral emission of laser-induced plasma from polymer," Appl. Surf. Sci. **255**, 9566–9571 (2009).
23. Q. Ma and P. Dagdigian, "Kinetic model of atomic and molecular emissions in laser-induced breakdown spectroscopy of organic compounds," Anal. Bioanal. Chem. **400**, 3193–3205 (2011).
24. S. Yuasa, Y. Zhu, and S. Sogo, "Ignition and combustion of aluminum in oxygen/nitrogen mixture streams," Combust. Flame **108**, 387–390 (1997).
25. A. Fontijn and W. Felder, "HTFFR kinetics studies of Al + CO_2 → AlO + CO from 300 to 1900 K, a non-Arrhenius reaction," J. Chem. Phys. **67**, 1561–1569 (1977).
26. D. R. Lide, ed., *Handbook of Chemistry and Physics*, 75th ed. (CRC Press, 1994).
27. J. Akhavan, *The Chemistry of Explosives*, 2nd ed. (The Royal Society of Chemistry, 2004).
28. Z. Ji and L. Shufen, "Aluminum oxidation in nitramine propellant," Propellants Explos. Pyrotech. **24**, 224–226 (1999).
29. K. Park, D. Lee, A. Rai, D. Mukherjee, and M. R. Zachariah, "Size-resolved kinetic measurements of aluminum nanoparticle oxidation with single particle mass spectrometry," J. Phys. Chem. B **109**, 7290–7299 (2005).
30. I. Balchev, N. Minkovski, T. Marinova, M. Shipochka, and N. Sabotinov, "Composition and structure characterization of aluminum after laser ablation," Mater. Sci. Eng. B **135**, 108–112 (2006).
31. C. S.-C. Yang, E. E. Brown, U. H. Hommerich, S. B. Trivedi, A. C. Samuels, and A. P. Snyder, "Mid-infrared emission from laser-induced breakdown spectroscopy," Appl. Spectrosc. **61**, 321–326 (2007).

NO. OF COPIES	ORGANIZATION
1 (PDF)	DEFENSE TECHNICAL INFORMATION CTR DTIC OCA 8725 JOHN J KINGMAN RD STE 0944 FORT BELVOIR VA 22060-6218
1 (PDF)	DIRECTOR US ARMY RESEARCH LAB RDRL CIO LL 2800 POWDER MILL RD ADELPHI MD 20783-1197
1 (PDF)	GOVT PRINTG OFC A MALHOTRA 732 N CAPITOL ST NW WASHINGTON DC 20401
1 (PDF)	RDRL WML B J GOTTFRIED